

Influence of curvature on the demagnetizing field of a ferromagnetic nanowire

V. L. Carvalho-Santos*

*Instituto Federal de Educação, Ciência e Tecnologia Baiano - Campus Senhor do Bonfim,
Km 04 Estrada da Igara, 48970-000 Senhor do Bonfim, Bahia, Brazil*

Abstract

Magnetic nanowires have been considered to compose devices based on the concepts of spintronic and magnonic technologies. Despite stripe and cylindrical nanomagnets being widely studied, curvature effects on the magnetic properties of nanowires have been low explored. In this work the analysis of the influence of curvature on the demagnetizing field inside a curved magnetic wire is proposed. By performing analytical calculations, it is shown that unlike their cylindrical counterparts, curved nanowires present a demagnetizing field that has different values along its polar-like angle. In addition, the demagnetizing field presents a dependence on the azimuthal position.

I. INTRODUCTION

Due to their potential applications in random access memory, data storage¹, cancer therapy², spintronic and magnonic devices³, magnetic nanoparticles have been widely studied, as from experimental as from theoretical point of view. From experimental point of view, several works have reported the production and characterization of nanomagnets with different shapes and sizes⁴⁻⁶. For instance, recent advances in experimental techniques to fabricate nanoparticles has made it possible the production of nanomagnets with unusual geometries such as rolled-up magnetic membranes⁷, paraboloidal magnetic caps⁸ or modulated nanomagnets⁹. The production of nanomagnets with cylindrical geometry (nanowires and nanotubes) has been also reported¹⁰. Such magnetic nanowires and nanotubes appear as prominent candidates to compose units of information for non-volatile memories, logic gates^{11,12} and devices based on the concept of “race-track memory”¹³. This development on experimental techniques to produce magnetic nanoparticles and the possibilities of applications for such structures make it necessary the understanding on the influence of curvature on the magnetic properties of nanoparticles. In this context, in last years, a lot of effort has been done aiming to describe how the geometry can influence the properties of nanomagnets^{20,21}.

The proposition of a race-track device demands the understanding on the dynamics of a domain wall along a nanowire. In the case of cylindrical nanowires, the knowledge on the dynamics of domain wall under the action of magnetic fields or spin currents is reasonably well developed¹⁴⁻¹⁷. Among main results, interesting properties appearing due to the symmetry of cylindrical nanowires are theoretically predicted and experimentally observed. Among them, the absence of a Walker field¹⁸ in the domain wall motion can be highlighted. Indeed, unlike what it is noted for stripe nanowires¹⁹, the domain wall moves smoothly in a cylindrical nanowire and its velocity does not present the oscillatory behavior occurring above the Walker field¹⁵. On the other hand, due to the lost of cylindrical symmetry, interesting magnetic properties are noted if the cylindrical nanowire is curved. For example, it was shown that a domain wall can be pinned even when it is passing across curved region of a nanowire²². In addition, torsion and curvature effects lead to the appearance of a Walker limit and negative velocities during the domain wall motion^{23,24}. Based on the above and on the influence of the geometry on the magnetic properties of nanomagnets, in this work

it is proposed the study of the dependence of the demagnetizing field on the geometry of a curved nanowire. It is well known that the demagnetizing field of an in-plane single domain state in a cylindrical nanowire is independent on the direction in which the magnetization is pointing in²⁵. On the other hand, once the cylindrical symmetry is lost in a curved wire, the demagnetizing field of a homogeneous magnetization configuration must present a dependence on the curvature. Indeed, by representing a curved wire as a torus section, the demagnetizing fields of four different magnetization configurations are obtained and it is shown that the components of the demagnetizing field present an explicit dependence on the curvature.

This work is divided as follows: in Section II we present the adopted theoretical model to describe the nanowire and to calculate the demagnetizing field; Section III brings the results and discussions; finally, in Section IV the conclusions and prospects are presented.

II. THEORETICAL MODEL

The main objective of this work is to determine the demagnetizing field generated inside a curved wire described as a torus section. In this case, the micromagnetic theory will be adopted. In the frame of micromagnetism, a magnetic structure is described as a continuous medium whose magnetic state is defined by the magnetization vector as a function of the position inside the element. In this case, the demagnetizing field can be calculated by $\mathbf{H} = -\nabla\Phi$, where Φ is the magnetostatic potential, determined from the Laplace equation $\nabla^2\Phi = 0$. In the absence of electric currents, the magnetostatic potential comes from surface and volumetric magnetic charges, respectively defined as $\sigma = \mathbf{m} \cdot \mathbf{n}$ and $\varrho = \nabla \cdot \mathbf{m}$. Here, \mathbf{n} is the normal vector pointing outward the surface of the magnet and $\mathbf{m} = \vec{M}/M_S$, with \mathbf{M} being the magnetization vector and M_S the saturation magnetization. In this case, the formal solution of the Laplace equation is given by

$$\Phi = \frac{M_S}{4\pi} \left[\int_S \frac{\sigma}{|\vec{r} - \vec{r}'|} dS - \int_V \frac{\varrho}{|\vec{r} - \vec{r}'|} dV \right], \quad (1)$$

where $|\vec{r}' - \vec{r}|$ is the distance between two points into the magnetic body.

Since a curved magnet is being considered, all vector operators must be given in a curvilinear basis²⁶. Then, in order to calculate the magnetostatic potential of a curved wire, it

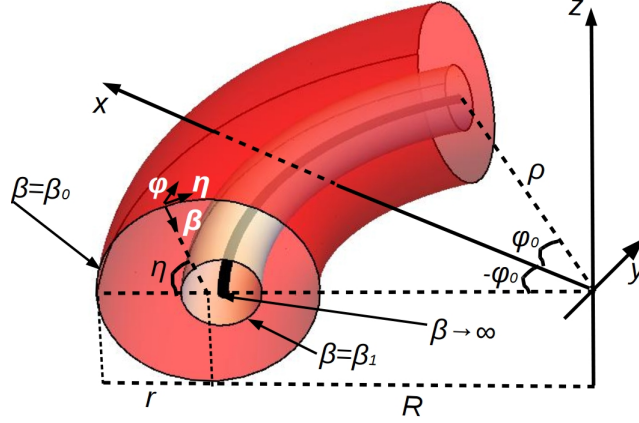


FIG. 1. Adopted coordinate system to describe the curved wire.

will be parametrized by a torus section, that is²⁷

$$\vec{r} = \hat{x} \frac{\rho \sinh \beta \cos \varphi}{\cosh \beta - \cos \eta} + \hat{y} \frac{\rho \sinh \beta \sin \varphi}{\cosh \beta - \cos \eta} + \hat{z} \frac{\rho \sin \eta}{\cosh \beta - \cos \eta}, \quad (2)$$

where ρ is a constant that defines the radius of a circle in the plane $z = 0$ when $\beta \rightarrow \infty$. $\beta \in [\beta_0, \infty)$ determines the torus thickness (β_0 describes the external surface), $\varphi \in [-\varphi_0, \varphi_0]$ plays the role of an azimuthal angle and $\eta \in [0, 2\pi]$ is the poloidal angle (See Fig. 1). The coordinate system represented in Eq. (2) can be related to a more natural parameters describing a torus by $\cosh \beta = R/r$ (the external surface of the wire is described by $\cosh \beta_0 = R/r$) and $\rho = \sqrt{R^2 - r^2}$, where r and R are the poloidal and toroidal radii²⁸, respectively. The wire length is given by $\ell = 2\varphi_0 R$ in such way that the wire with greater curvature, described by a half-torus section, is obtained when ($\varphi_0 = \pi/2 \rightarrow R = \ell/\pi$) and an almost straight wire is obtained for $R \rightarrow \infty$. From Eq. (2), one can evaluate the normal vector pointing outward the wire surface, obtaining $\mathbf{n} = -\hat{\beta} = -F(\beta, \eta)\hat{R} - G(\beta, \eta)\hat{z}$, where

$$F(\beta, \eta) \equiv F = \frac{1 - \cosh \beta \cos \eta}{\cosh \beta - \cos \eta} \quad (3)$$

and

$$G(\beta, \eta) \equiv G = -\frac{\sinh \beta \sin \eta}{\cosh \beta - \cos \eta}. \quad (4)$$

In addition, $\hat{R} = \hat{x} \cos \varphi + \hat{y} \sin \varphi$ is the radial vector pointing outward the wire in the xy -plane.

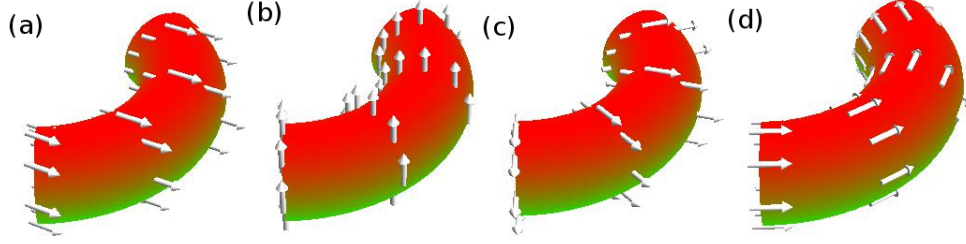


FIG. 2. Considered magnetization configurations. (a) describes a SDx state; (b) a SDz state; (c) represents a RSD state; and (d), a VSD state.

The magnetization $\vec{M} \equiv M_S \mathbf{m}$ is parametrized in a spherical coordinate system (r, ϕ, θ) on the basis of Cartesian coordinates, that is, $\mathbf{m} = \hat{x} \cos \phi \sin \theta + \hat{y} \sin \phi \sin \theta + \hat{z} \cos \theta$. For the purposes of this work, the demagnetizing fields associated with four different magnetization configurations (see Fig. 2) will be calculated: i) a single domain state pointing along x direction (SDx), described by $\mathbf{m}_{SDx} = \hat{x}$; ii) a single domain state pointing along z -axis direction (SDz), where $\mathbf{m}_{SDz} = \hat{z}$; iii) a radial single domain state (RSD), in which the magnetic moments pointing outward the wire and are described by $\mathbf{m}_{RSD} = \hat{R}$; and an in-surface state (HV), in which the magnetic moments point along azimuthal direction of the wire, $\mathbf{m}_{HV} = \hat{\phi} = -\hat{x} \sin \phi + \hat{y} \cos \phi$. These magnetic states have been chosen because they share general features of other magnetic configurations that can appear as magnetization groundstate or metastable states in a curved nanowire.

The calculation of the magnetostatic potential is, in general, very hard. A possible way is expanding the inverse of the distance in an infinite series using Green's functions. In the case of toroidal geometry, the inverse of the distance in toroidal coordinates is given by²⁷

$$\frac{1}{|\vec{r}' - \vec{r}|} = \frac{\sqrt{(\cosh \beta' - \cos \eta')(\cosh \beta - \cos \eta)}}{\pi \rho} \sum_{k,n=0}^{\infty} (-1)^k \varepsilon_n \varepsilon_k \cos n(\eta' - \eta) \times \cos k(\varphi' - \varphi) \frac{\Gamma(n-k+1/2)}{\Gamma(n+k+1/2)} P_{n-1/2}^k(\cosh \beta_{<}) Q_{n-1/2}^k(\cosh \beta_{>}), \quad (5)$$

where $\varepsilon_k = (2 - \delta_{k,0})$, $\varepsilon_n = (2 - \delta_{n,0})$, $\Gamma(x)$ is the gamma function, $P_{n-1/2}^k(\cosh \beta)$ and $Q_{n-1/2}^k(\cosh \beta)$ are the Legendre functions of half-integer order (also known as toroidal harmonics). From using the expansion given in Eq. (5), the magnetostatic potential for single domain²⁹ and onion³⁰ states in magnetic nanotori were obtained.

In some situations, it is useful to describe the components of a vector field in their Cartesian components. In this context, the components of a vector field (\mathbf{H}) written in

toroidal coordinates (β, η, φ) can be changed to a Cartesian basis (x, y, z) by using the transformation

$$\begin{pmatrix} H_x \\ H_y \\ H_z \end{pmatrix} = \begin{pmatrix} F \cos \varphi & G \cos \varphi & -\sin \varphi \\ F \sin \varphi & G \sin \varphi & \cos \varphi \\ G & -F & 0 \end{pmatrix} \begin{pmatrix} H_\beta \\ H_\eta \\ H_\varphi \end{pmatrix}, \quad (6)$$

where F and G were defined in Eq. (3).

III. RESULTS

From the presented model, analytical expressions for the magnetostatic potential and the demagnetizing fields associated to each magnetization configuration can be determined.

A. Magnetostatic potential

There are two contributions to the magnetostatic potential associated to SDx state. The first contribution comes from the ends of the wire, that is, at $-\varphi_0$ (S_1) and φ_0 (S_2), where $\mathbf{m}_{SDx} \cdot \hat{\varphi} = -\sin \varphi_0$. The second contribution comes from magnetostatic charges appearing along the wire external surface (β_0) and given by $\mathbf{m}_{SDx} \cdot \mathbf{n} = -F \cos \varphi$. Thus, the magnetostatic potential of SDx is given by $\Phi_{SDx} = \Phi_{SDx1} + \Phi_{SDx2}$, where

$$\Phi_{SDx1} = -\frac{M_S}{4\pi} \left\{ \int_{S_1} \frac{\sin \varphi_0}{|\vec{r}' - \vec{r}|} dS_1 + \int_{S_2} \frac{\sin \varphi_0}{|\vec{r}' - \vec{r}|} dS_2 \right\}, \quad (7)$$

and

$$\Phi_{SDx2} = \frac{M_S}{4\pi} \int_{S_3} \frac{1}{|\vec{r}' - \vec{r}|} \left[\frac{\cos \varphi (\cosh \beta_0 \cos \eta - 1)}{(\cosh \beta_0 - \cos \eta)} \right] dS_3, \quad (8)$$

where the integrals are evaluated at the wire surface. The surface element along the wire external surface is $dS_3 = \rho^2 \sinh \beta_0 / (\cosh \beta_0 - \cos \eta)^2 d\eta d\varphi$, while the surface element at the wire ends is $dS_1 = dS_2 = \rho^2 / (\cosh \beta - \cos \eta)^2 d\eta d\beta$.

The integral in φ must be evaluated in the interval $\varphi \in [-\varphi_0, \varphi_0]$. In this case, the substitution of Eq. (5) in Eqs. (7) and (8) yields

$$\begin{aligned} \frac{\Phi_{SDx1}}{M_S} = & -\frac{\rho \sqrt{\cosh \beta' - \cos \eta'}}{2\pi^2} \sum_{k,n=0}^{\infty} (-1)^k \varepsilon_n \varepsilon_k g_k(\varphi') P_{n-1/2}^k(\cosh \beta') \\ & \times \int_{\beta_0}^{\infty} d\beta Q_{n-1/2}^{-k}(\cosh \beta) \int_0^{2\pi} d\eta \frac{\cos n(\eta - \eta')}{(\cosh \beta - \cos \eta)^{3/2}}, \end{aligned} \quad (9)$$

and

$$\begin{aligned} \frac{\Phi_{SDx2}}{M_S} &= \frac{\rho \sinh \beta_0 \sqrt{\cosh \beta' - \cos \eta'}}{4\pi^2} \sum_{k,n=0}^{\infty} (-1)^k \varepsilon_n \varepsilon_k f_k(\varphi') P_{n-1/2}^k(\cosh \beta_0) \\ &\quad \times Q_{n-1/2}^{-k}(\cosh \beta) \int_0^{2\pi} d\eta \frac{\cos n(\eta - \eta') (\cosh \beta_0 \cos \eta - 1)}{(\cosh \beta_0 - \cos \eta)^{5/2}}, \end{aligned} \quad (10)$$

where $g_k(\varphi') = \sin \varphi_0 \cos k\varphi_0 \cos k\varphi'$,

$$f_k(\varphi') = \frac{2 \cos k\varphi' (k \sin k\varphi_0 \cos \varphi_0 - \cos k\varphi_0 \sin \varphi_0)}{k^2 - 1}. \quad (11)$$

and we have used the property³¹

$$\frac{\Gamma(n - k + 1/2)}{\Gamma(n + k + 1/2)} Q_{n-1/2}^k(\cosh \beta') = Q_{n-1/2}^{-k}(\cosh \beta'), \quad (12)$$

The integrals in η can be performed from using the trigonometric identity $\cos n(\eta' - \eta) = \cos n\eta \cos n\eta' + \sin n\eta \sin n\eta'$ and the integral representation of $Q_{n-1/2}^k(\cosh \beta)$ (See Ref.²⁷ p. 961). In this case, after some algebraic manipulation, we have that

$$\Phi_{SDx1} = \sqrt{\cosh \beta' - \cos \eta'} \sum_{k,n=0}^{\infty} \cos n\eta' \Omega_{k,n}(\beta_0) g_k(\varphi') P_{n-1/2}^k(\cosh \beta'), \quad (13)$$

and

$$\Phi_{SDx2} = \sqrt{\cosh \beta' - \cos \eta'} \sum_{k,n=0}^{\infty} \cos n\eta' \Lambda_{k,n}(\beta_0) f_k(\varphi') Q_{n-1/2}^{-k}(\cosh \beta'), \quad (14)$$

where

$$\Omega_{k,n}(\beta_0) = \frac{2\rho M_S \sqrt{2}}{\pi^2} (-1)^k \varepsilon_n \varepsilon_k \int_{\beta_0}^{\infty} d\beta \frac{Q_{n-1/2}^{-k}(\cosh \beta) Q_{n-1/2}^1(\cosh \beta)}{\sinh \beta}, \quad (15)$$

and

$$\begin{aligned} \Lambda_{k,n}(\beta_0) &= -\frac{2\rho M_S \sqrt{2} \cosh \beta_0}{3\pi^2} (-1)^k \varepsilon_n \varepsilon_k P_{n-1/2}^{k\ 0} \\ &\quad \times \left[\frac{Q_{n+1/2}^{2\ 0}}{\sinh \beta_0} - n Q_{n-1/2}^{1\ 0} - \frac{Q_{n-1/2}^{2\ 0}}{\sinh \beta_0} \right], \end{aligned} \quad (16)$$

with $P(Q)_{\nu}^{\mu\ 0} \equiv P(Q)_{\nu}^{\mu}(\cosh \beta_0)$.

The calculation of the magnetostatic potential of the SDz configuration follows the same procedure above described. However, in this case, the ends of the wire do not contribute to the magnetostatic potential. Thus, the magnetostatic potential of this configuration is

$$\Phi_{SDz} = \frac{M_S}{4\pi} \int_{S_3} \frac{\rho^2 \sinh \beta}{|\vec{r}' - \vec{r}|} \left[\frac{\sinh \beta \sin \eta}{(\cosh \beta - \cos \eta)^3} \right] d\eta d\varphi. \quad (17)$$

Then, analogously to the performed calculations to determine Φ_{SDx2} , we have that

$$\Phi_{SDz} = \sqrt{\cosh \beta' - \cos \eta'} \sum_{k,n=0}^{\infty} n \sin n\eta' \Psi_{k,n}(\beta_0) h_k(\varphi') Q_{n-1/2}^{-k}(\cosh \beta'), \quad (18)$$

where

$$\Psi_{k,n}(\beta_0) = -\frac{8\rho M_S \sqrt{2} \sinh \beta_0}{3\pi^2} (-1)^k \varepsilon_n \varepsilon_k Q_{n-1/2}^1 P_{n-1/2}^k \quad (19)$$

and $h_k(\varphi') = k^{-1}(2 \cos k\varphi' \sin k\varphi_0)$.

The third configuration consists in a radial state. As the SDz state, RSD has no surface magnetostatic charges at the ends of the wire. However, there are two contributions to the magnetostatic potential. One coming from surface and other coming from volumetric charges. That is, $\Phi_{RSD} = \Phi_{RSD_S} + \Phi_{RSD_V}$, where subscripts S and V denote surface and volumetric contributions to the magnetostatic potential. From the definition of the magnetization in RSD state, it can be noted that $\mathbf{m}_{RSD} \cdot \mathbf{n} = -F$. Then, the calculation of the surface contribution to the magnetostatic potential is promptly obtained from the expression of Φ_{SDx2} with the replacement of $f_k(\varphi')$ by $h_k(\varphi')$. Then,

$$\Phi_{RSD_S} = \sqrt{\cosh \beta' - \cos \eta'} \sum_{k,n=0}^{\infty} \cos n\eta' \Lambda_{k,n}(\beta_0) h_k(\varphi') Q_{n-1/2}^{-k}(\cosh \beta'). \quad (20)$$

The volumetric charge associated to RSD state is determined from the divergent of the magnetization written in curvilinear coordinate system²⁶, $\nabla \cdot \mathbf{m}_{RSD} = (\cosh \beta - \cos \eta)/\rho \sinh \beta$. Therefore, after some algebraic manipulation, the following expression is obtained

$$\begin{aligned} \Phi_{RSD_V} &= \frac{\rho M_S \sqrt{2}}{\pi^2} \sqrt{\cosh \beta' - \cos \eta'} \sum_{k,n=0}^{\infty} (-1)^k \varepsilon_n \varepsilon_k \cos n\eta' \\ &\times h_k(\varphi') P_{n-1/2}^k(\cosh \beta') \int_{\beta_0}^{\infty} \frac{Q_{n-1/2}^1(\cosh \beta) Q_{n-1/2}^{-k}(\cosh \beta)}{\sinh \beta} d\beta \\ &\Rightarrow \Phi_{RSD_V} = \frac{1}{2} \sqrt{\cosh \beta' - \cos \eta'} \sum_{k,n=0}^{\infty} \cos n\eta' \Omega_{k,n}(\beta_0) \\ &\times h_k(\varphi') P_{n-1/2}^k(\cosh \beta'). \end{aligned} \quad (21)$$

At last, it will be analyzed the magnetostatic potential of a VSD configuration. In this case, only the surface charges associated to the ends of the wire accounts to the calculations and thus, the magnetostatic potential of VSD state is given by

$$\Phi_{VSD} = -\frac{\Phi_{SDx1}}{\sin \varphi_0}. \quad (22)$$

B. Demagnetizing fields

Despite having analyzed the magnetostatic potential of four different magnetization configurations, due to their similar expressions, in this subsection only the demagnetizing field of RSD and SDz states will be evaluated. The results here obtained give a good qualitative description for the two other states.

By using the ∇ operator in toroidal coordinates²⁷, the demagnetizing field in a toroidal coordinate system is evaluated as

$$\mathbf{H}_d = -\frac{\cosh \beta' - \cos \eta'}{\rho} \left[\frac{\partial \Phi}{\partial \beta'} \hat{\beta}' + \frac{\partial \Phi}{\partial \eta'} \hat{\eta}' + \frac{1}{\sinh \beta'} \frac{\partial \Phi}{\partial \varphi'} \hat{\varphi}' \right]. \quad (23)$$

Therefore, the demagnetizing field in a toroidal basis can be represented as $\mathbf{H}_d = H_\beta \hat{\beta} + H_\eta \hat{\eta} + H_\varphi \hat{\varphi}$. In this case, the components of the demagnetizing field associated to surface charges of RSD state are given by

$$H_{\beta_{RSD}}^S = -\frac{\sqrt{\cosh \beta - \cos \eta}}{\rho} \sum_{k,n=0}^{\infty} \cos n\eta \Lambda_{k,n}(\beta_0) h_k(\varphi) \times \left\{ \frac{\sinh \beta}{2} Q_{n-1/2}^{-k}(\cosh \beta) + (\cosh \beta - \cos \eta) \frac{dQ_{n-1/2}^{-k}(\cosh \beta)}{d\beta} \right\}, \quad (24)$$

$$H_{\eta_{RSD}}^S = -\frac{\sqrt{\cosh \beta - \cos \eta}}{\rho} \sum_{k,n=0}^{\infty} \Lambda_{k,n}(\beta_0) h_k(\varphi) Q_{n-1/2}^{-k}(\cosh \beta) \times \left\{ \frac{1}{2} \sin \eta \cos n\eta - n(\cosh \beta - \cos \eta) \sin n\eta \right\}, \quad (25)$$

and

$$H_{\varphi_{RSD}}^S = -\frac{(\cosh \beta - \cos \eta)^{3/2}}{\rho \sinh \beta} \sum_{k,n=0}^{\infty} \cos n\eta \Lambda_{k,n}(\beta_0) Q_{n-1/2}^{-k}(\cosh \beta) \frac{dh_k(\varphi)}{d\varphi}. \quad (26)$$

The components of the demagnetizing field associated to the volumetric charges of RSD configuration are

$$H_{\beta_{RSD}}^V = -\frac{\sqrt{\cosh \beta - \cos \eta}}{2\rho} \sum_{k,n=0}^{\infty} \cos n\eta \Omega_{k,n}(\beta_0) h_k(\varphi) \times \left\{ \frac{\sinh \beta}{2} P_{n-1/2}^k(\cosh \beta) + (\cosh \beta - \cos \eta) \frac{dP_{n-1/2}^k(\cosh \beta)}{d\beta} \right\}, \quad (27)$$

$$H_{\eta_{RSD}}^V = -\frac{\sqrt{\cosh \beta - \cos \eta}}{2\rho} \sum_{k,n=0}^{\infty} \Omega_{k,n}(\beta_0) h_k(\varphi) P_{n-1/2}^k(\cosh \beta) \times \left\{ \frac{1}{2} \sin \eta \cos n\eta - n(\cosh \beta - \cos \eta) \sin n\eta \right\}, \quad (28)$$

and

$$H_{\varphi_{RSD}}^V = -\frac{(\cosh \beta - \cos \eta)^{3/2}}{2\rho \sinh \beta} \sum_{k,n=0}^{\infty} \cos n\eta \Omega_{k,n}(\beta_0) P_{n-1/2}^k(\cosh \beta) \frac{dh_k(\varphi)}{d\varphi}. \quad (29)$$

Since the magnetostatic potential of SDx configuration (Eqs. (10) and (14)) has similar expressions to the magnetostatic potential of RSD state (Eqs. (20) and (21)), qualitative behavior of the demagnetizing field for SDx state is well described by the previously presented results. Then, explicit equations of the demagnetizing field associated with SDx configuration will be omitted here.

The solution of the magnetostatic potential of SDz state (See Eq. (18)) presents subtle differences when compared with Eq. (20). In this context, it is interesting to perform the explicit calculation of the demagnetizing field related to this configuration, which is evaluated as

$$H_{\beta_{SDz}} = -\frac{\sqrt{\cosh \beta - \cos \eta}}{\rho} \sum_{k,n=0}^{\infty} n \sin n\eta \Psi_{k,n}(\beta_0) h_k(\varphi) \times \left\{ \frac{\sinh \beta}{2} Q_{n-1/2}^{-k}(\cosh \beta) + (\cosh \beta - \cos \eta) \frac{dQ_{n-1/2}^{-k}(\cosh \beta)}{d\beta} \right\}, \quad (30)$$

$$H_{\eta_{SDz}} = -\frac{\sqrt{\cosh \beta - \cos \eta}}{\rho} \sum_{k,n=0}^{\infty} n \Psi_{k,n}(\beta_0) h_k(\varphi) Q_{n-1/2}^{-k}(\cosh \beta) \times \left\{ \frac{1}{2} \sin \eta \sin n\eta + n(\cosh \beta - \cos \eta) \cos n\eta \right\}, \quad (31)$$

and

$$H_{\varphi_{SDz}} = -\frac{(\cosh \beta - \cos \eta)^{3/2}}{\rho \sinh \beta} \sum_{k,n=0}^{\infty} n \sin n\eta \Psi_{k,n}(\beta_0) Q_{n-1/2}^{-k}(\cosh \beta) \frac{dh_k(\varphi)}{d\varphi}. \quad (32)$$

C. Numerical results

Despite having obtained analytical expressions for the demagnetizing field components given in Eqs. (24)-(32), an immediate analysis of their physical content is not clear due to their complicated forms. Therefore, to extract relevant results we should evaluate them numerically. For doing that, we employ the Fortran subroutine code DTORH1^{32,33}, which gives the values of $P_{n-1/2}^k(\cosh \beta)$ and $Q_{n-1/2}^k(\cosh \beta)$. Due to the fast convergence of the series, we stop the sums at $k = 30$ and $n = 30$.

In this work, the results are normalized in relation to the saturation magnetization, that is, in numerical calculations $M_S = 1$ is adopted. In addition, the poloidal radius and length of the nanowires are respectively $r = 10$ nm and $\ell = 100$ nm. The toroidal radius R is varied in function of φ_0 , in the form $R = \ell/2\varphi_0$. Consequently, the wire with greater curvature, $K = 1/R = \pi \times 10^7 m^{-1}$, is given by a half-torus section ($\varphi_0 = \pi/2$). The presented numerical results describe the demagnetizing field on the wire surface ($\beta = \beta_0$).

Figs. 3-(a) and (b) present respectively the dependence of $H_{\beta_{RSD}}$ on the curvature and on the azimuthal position, φ , along the wire. From Fig.3a, it can be noted that $H_{\beta_{RSD}}$ depends on the curvature of the wire. In this case, the graphics show a cosine-like behavior and an asymmetry for $\eta = 0$ and $\eta = \pi$ is observed. That is, the absolute value of $H_{\beta_{RSD}}$ at $\eta = 0$ is lower than its absolute value at $\eta = \pi$. Then, $\Delta H_{\beta_{RSD}} = H_{\beta_{RSD}\eta=0} - H_{\beta_{RSD}\eta=\pi} < 0$. Nevertheless, it is interesting to note that the smaller the curvature, the smaller $\Delta H_{\beta_{RSD}}$, in such way that $\Delta H_{\beta_{RSD}} \rightarrow 0$ when $1/K \rightarrow 0$. On the other hand, despite small quantitative variations, qualitative changes of $H_{\beta_{RSD}}$ are no observed at different positions along the wire (See Fig. 3-(b)). Figs. 3-(c) and (d) present the behavior of $H_{\eta_{RSD}}$ for different curvatures and different positions along the wire. It can be noted a sine-like behavior with maxima absolute values given at $\eta = \pi/2$ and $\eta = 3\pi/2$. Despite $H_{\eta_{RSD}}$ is depending on curvature, no asymmetry is observed when we compare its maximum absolute values at $\eta = \pi/2$ and $\eta = 3\pi/2$. Finally, the behavior of $H_{\varphi_{RSD}}$ in function of the position along the wire is shown in Fig. 3-(f). It can be noted that $H_{\varphi_{RSD}} = 0$ in the center of the wire ($\varphi = 0$) and increases, in absolute value, reaching its maximum value at the wire ends. The maximum value of the demagnetizing field appearing in the internal border of the wire shows an interesting relation between curvature and dipolar energy. This effect must be important in describing the properties of a domain wall displacing along curved wires. However, curvature effects on the dypolar field is a low explored issue. In general, most of works devoted to study this theme use the space of momenta to calculate the demagnetizing field of curved particles³⁴⁻³⁷.

In Fig. 4 it is presented the components of the demagnetizing fields of SDz configuration, obtained from Eqs. (30) - (32). Analogously to what happens for RSD state, the demagnetizing field depends on the curvature of the wire. However, there is a reversal in the behavior of H_β and H_η . That is, $H_{\beta_{SDz}}$ presents a sine-like behavior and its absolute value is symmetric under the change from $\eta = \pi/2$ to $\eta = 3\pi/2$. On the other hand, $H_{\eta_{SDz}}$ presents a cosine-like behavior with a maximum value (in absolute value) at $\eta = \pi$.

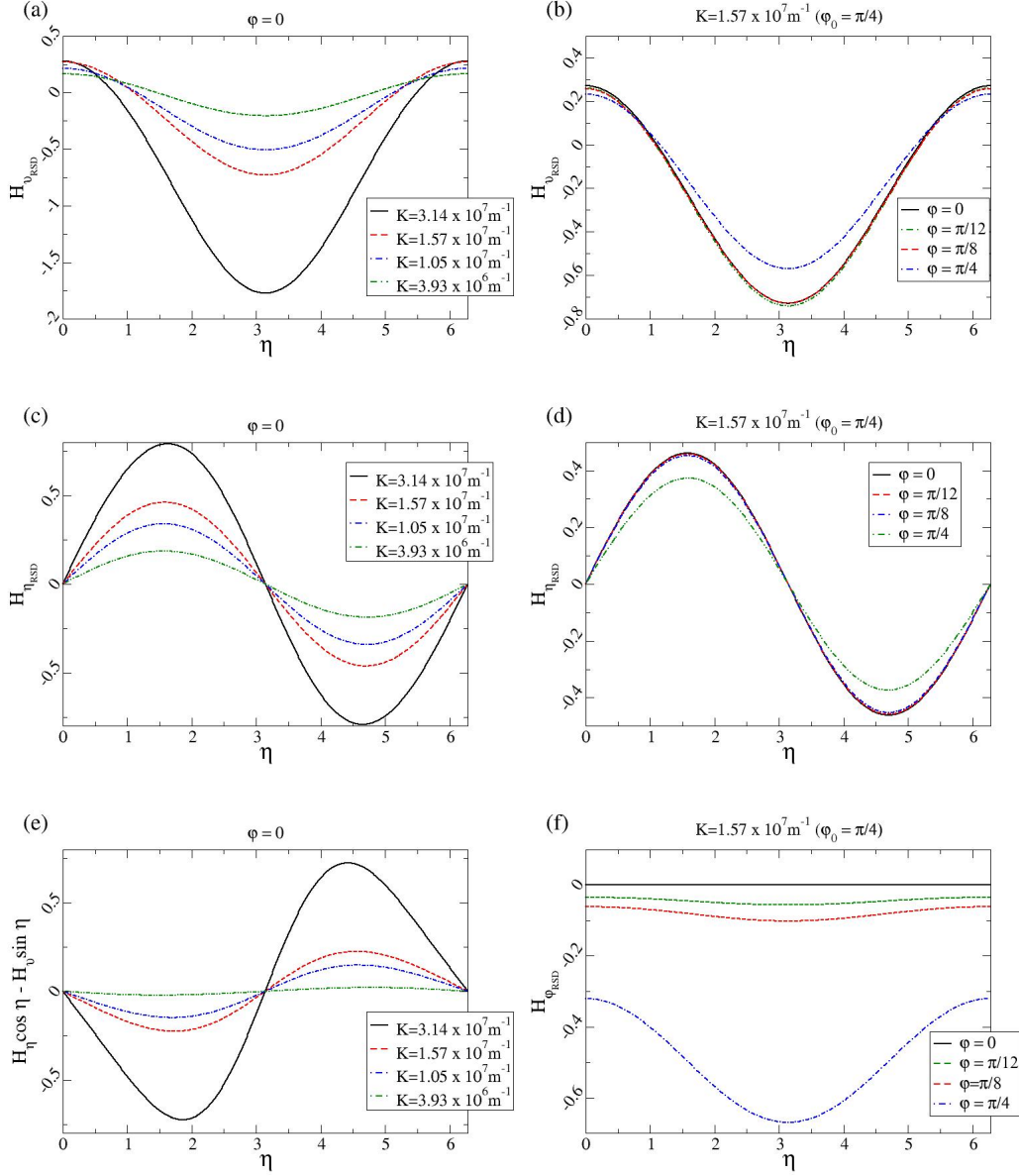


FIG. 3. Components of the demagnetizing field of RSD state for different curvatures and azimuthal positions along the curved wire in function of η . (a) and (c) show, respectively, $H_{\beta_{RSD}}$ and $H_{\eta_{RSD}}$ at $\varphi = 0$ for different curvatures. (b) and (d) show the dependence of $H_{\beta_{RSD}}$ and $H_{\eta_{RSD}}$ on the azimuthal position φ along the wire for a constant curvature. Fig. (e) shows the behavior of the function $f(\eta) = H_{\eta_{RSD}} \cos \eta - H_{\beta_{RSD}} \sin \eta$. (f) shows the dependence of $H_{\varphi_{RSD}}$ on the azimuthal position along the wire for a constant curvature.

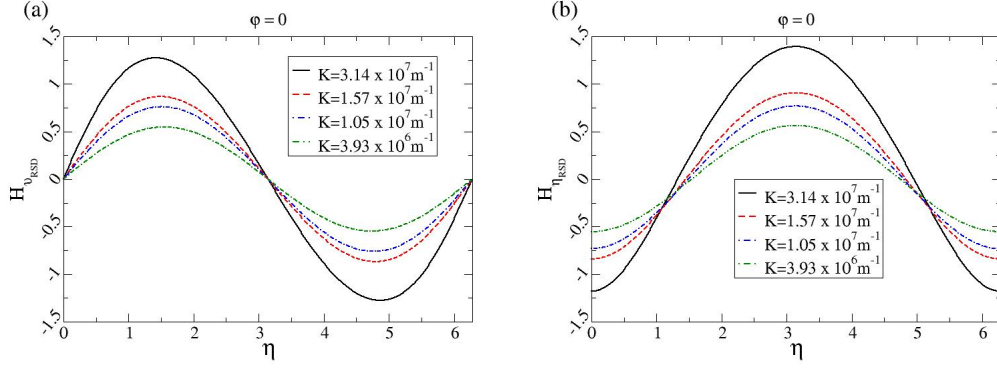


FIG. 4. Components of the demagnetizing field of SDz state for different curvatures in function of η . (a) shows the behavior of $H_{\beta_{SDz}}$ and (b) presents $H_{\eta_{SDz}}$ at $\phi = 0$ for different curvatures.

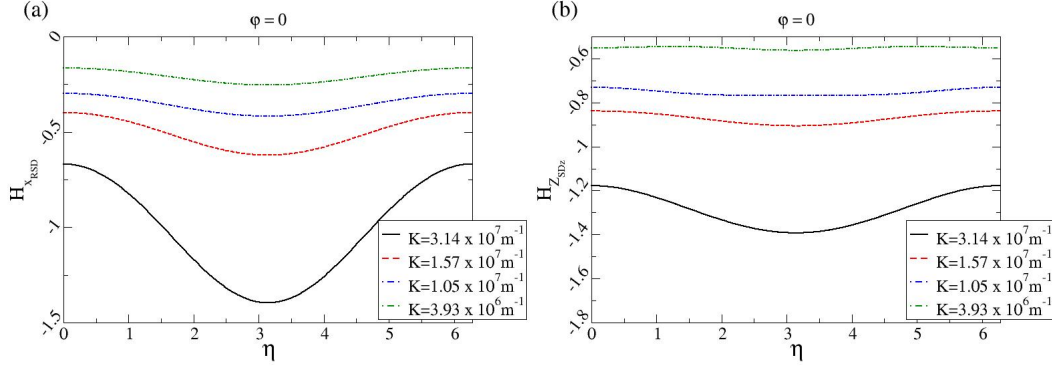


FIG. 5. Fig. (a) presents the component along x -axis direction in function of η for different curvatures. Fig. (b) shows the demagnetizing field pointing along z -axis direction for the SDz state.

The representation of the demagnetizing fields in a Cartesian basis can lead to a more intuitive description of the demagnetizing field of a curved wire. By using Eq. (6), we can numerically calculate the components $H_{x_{RSD}}$ and $H_{z_{SDz}}$. The analysis of Fig. 5 evidences the dependence on the curvature of the demagnetizing fields, as well as the maximum (absolute value) of the demagnetizing fields at $\eta = \pi$. It can be noted that $H_{x_{RSD}}$ decreases with the decreasing of curvature and its value tends to a constant for $1/K \rightarrow 0$. This behavior is noted also for $H_{z_{SDz}}$.

This curvature-dependent demagnetizing field can produce differences in the magnetization groundstate of nanowires when they are curved. Furthermore, a domain wall displacing

along a curved nanowire must present curvature-induced changes in its dynamics. In fact, Yershov *et al*²² showed that a domain wall can be pinned by a curved region in a cylindrical nanowire. However, in that work, the observed effects are purely related with exchange energy cost. Here, we show that dipolar field can also produce observable effects on the magnetic properties of a curved wire.

IV. CONCLUSIONS

Analytical solutions to the magnetostatic potential of four magnetization configurations (SDx, SDz, RSD and VSD) have been obtained by representing a curved wire as a torus section. For considering a curvilinear basis, the demagnetizing field of two of the considered configurations (RSD and SDz) have been explicitly calculated. The obtained results evidence a dependence of the demagnetizing field on the curvature of the wire. Furthermore, despite its angular symmetry along poloidal direction, the absolute values of the demagnetizing fields are different at the external and internal borders of the wire. The dependence on the curvature of the demagnetizing field is also evidenced when the demagnetizing field components are written in terms of a Cartesian basis. The obtained solutions are important to describe the magnetization groundstate configuration and the properties of a domain wall in a curved wire.

The author thanks the financial support of the Brazilian agencies CNPq (301015/2015-5) and Fapesb (JCB0063/2016). He thanks also D. Altbir and A. Espejo for fruitful discussions and suggestions.

* vagson.carvalho@usach.cl

¹ R. Hertel, Nat. Nanotechnol. 8, 318 (2013).

² D.-H. Kim, E. Rozhkova, I. Ulasov, S. Bader, T. Rajh, M. Lesniak, and V. Novosad, Nature Mater. 9, 165 (2009).

³ A.P. Guimarães, *Principles of Nanomagnetism*, (Springer, Heidelberg, 2009).

⁴ R. P. Cowburn, D. K. Koltsov, A. O. Adeyeye, M. E. Welland, D. M. Triker, Phys. Rev. Lett. **83**, 1042 (1999).

- ⁵ F. Q. Zhu, G.W. Chern, O. Thernyshyov, X.C. Zhu, J.G. Zhu, and C.L. Chien, Phys. Rev. Lett. **96**, 027205 (2006).
- ⁶ R. P. Cowburn, J. Phys. **D 33**, R1 (2000).
- ⁷ R. Streubel, D.J. Thurmer, D. Makarov, F. Kronast, T. Kosub, V.P. Kravchuk, D.D. Sheka, Y. Gaididei, R. Schfer, and O.G. Schmidt, Nano Lett. **12**, 3961 (2012).
- ⁸ D.W. Shi, P.K. Greene, P. Liu, K. Javed, K. Liu, and X. F. Han, IEEE Trans. on Magnetism **50**, 2303004 (2014).
- ⁹ I. Minguez-Bacho, S. Rodriguez-López, M. Vázquez, M. Hernández-Vélez, and K. Nielsch, Nanotechnology **25**, 145301 (2014).
- ¹⁰ M. Vázquez, in *Advanced Magnetic Nanowires* ed. by H. Kromüller, and S. Parkin, Handbook of Magnetism and Advanced Magnetic Materials, vol. 4 (Wiley, Chichester, 2007).
- ¹¹ J. Jaworowicz, N. Vernier, J. Ferré, A. Maziewski, D. Stanescu, D. Ravelosona, A.S. Jacqueline, C. Chappert, B. Rodmac, and B. Diény, Nanotechnology **20**, 215401 (2009).
- ¹² D.A. Allowood, G. Xiong, C.C. Faulkner, D. Atkinson, D. Petit, and R.P. Cowburn, Science **309**, 1688 (2005)
- ¹³ S.S.P. Parkin, M. Hayashi, and L. Thomas, Science **320**, 190 (2008);
- ¹⁴ Y.P. Ivanov, M. Vázquez, and O. Chubykalo-Fesenko, J. Phys. D. **46**, 485001 (2013).
- ¹⁵ M. Yan, A. Kákay, S. Gliga, and R. Hertel, Phys. Rev. Lett. **104**, 057201 (2010).
- ¹⁶ R. Wieser, E.Y. Vedmedenko, P. Weinberger, and R. Wiesendanger, Phys. Rev. **B 82**, 144430 (2010).
- ¹⁷ R. Hertel, and A. Kákay, J. Magn. Mag. Mat. **379**, 45 (2015).
- ¹⁸ N.L. Schryer, and L.R. Walker, J. Appl. Phys. **45**, 5406 (1974).
- ¹⁹ A. Mougin, M. Cormier, J.P. Adam, P.J. Metaxas, and J. Ferré, Europhys. Lett. **78**, 57007 (2007).
- ²⁰ Y. Gaididei, V.P. Kravchuk, and D.D. Sheka, Phys. Rev. Lett. **112**, 257203 (2014).
- ²¹ R. Streubel, P. Fischer, F. Kronast, V.P. Kravchuk, D.D. Sheka, Y. Gaididei, O.G. Schmidt, and D. Makarov, J. Phys. **D 49**, 363001 (2016).
- ²² K.V. Yershov, V.P. Kravchuk, D.D. Sheka, and Y. Gaididei, Phys. Rev. **B 92**, 104412 (2015).
- ²³ K.V. Yershov, V.P. Kravchuk, D.D. Sheka, and Y. Gaididei, Phys. Rev. **B 93**, 094418 (2016).
- ²⁴ O.V. Pylypovskyi, D.D. sheka, V.P. Kravchuk, K.V. Yershov, D. Makarov, and Y. Gaididei, Sci. Rep. **6**, 23316 (2016).

- ²⁵ A. Aharoni, IEEE Trans. on Magnetism **27**, 3539 (1991); L. Kraus, Czech. J. Phys. **B 23**, 512 (1973).
- ²⁶ G.B. Arfken, and H.J. Weber, *Mathematical Methods for Physicists*, 6th ed. (Elsevier Academic Press, 2005).
- ²⁷ P. Morse, and H. Feshbach, *Methods of Theoretical Physics*, (M Graw-Hill, New York, 1953).
- ²⁸ S. Vojkovic, A.S. Nunez, D. Altbir, and V.L. Carvalho-Santos, J. Appl. Phys. **120**, 033901 (2016).
- ²⁹ M. Bellegia, M. De Graef, and Y.T. Millev, Proc. R. Soc. **A 465**, 3581 (2009).
- ³⁰ V.L. Carvalho-Santos, W.A. Moura-Melo, and A.R. Pereira, J. Appl. Phys. **108**, 094310 (2010).
- ³¹ I.S. Gradshteyn, and I.M. Ryzhik, *Table of Integral, Series and Products*, 7th ed. (Academic, New York, 2007).
- ³² J. Segura, and A. Gil, Comput. Phys. Commun. **124**, 104 (2000).
- ³³ J. Segura, and A. Gil, Comput. Phys. Commun. **139**, 186 (2001).
- ³⁴ M. Bellegia, J.W. Lau, M.A. Shofield, Y. Zhu, S. Tandon, M. De Grael, J. Magn. Mag. Mat. **301**, 131 (2006).
- ³⁵ M. Beleggia, M. De Graef, J. Magn. Mag. Mat. **263**, L1 (2003).
- ³⁶ S. Tandon, M. Beleggia, Y. Zhu, M. De Graef, J. Magn. Mag. Mat. **271**, 27 (2004).
- ³⁷ M. Beleggia, M. De Graef, J. Magn. Mag. Mat. **285**, L1 (2004).